

# EvTTC: An Event Camera Dataset for Time-to-Collision Estimation

Kaizhen Sun<sup>1,\*</sup>, Jinghang Li<sup>1,\*</sup>, Kuan Dai<sup>1</sup>, Bangyan Liao<sup>2</sup>, Wei Xiong<sup>3</sup> and Yi Zhou<sup>1,†</sup>

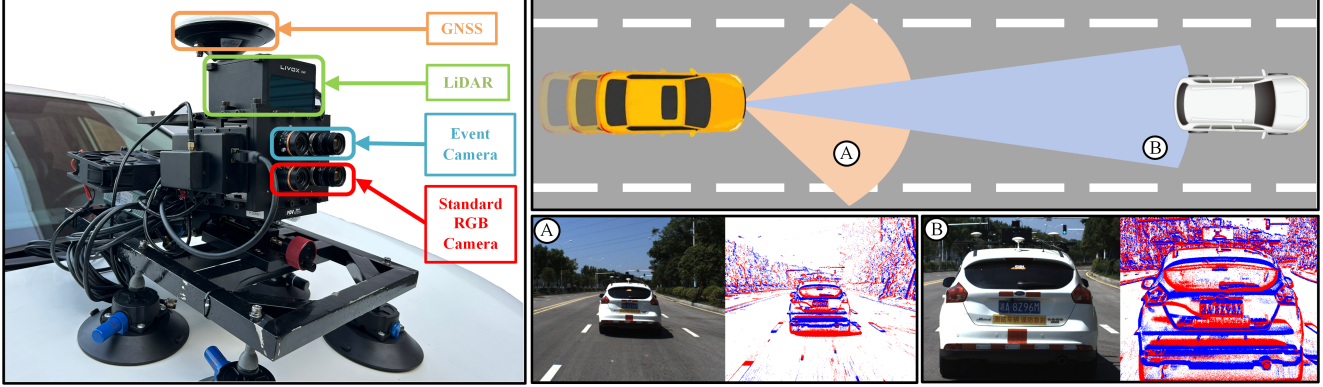


Fig. 1: Left: An overview of the data collection setup. Right: The top image shows a bird's-eye view of the vehicle on the highway, with fields of view and detection distances indicated by circled letters. The bottom row presents RGB images and accumulated event data captured by both the 8-mm Lens and 16-mm Lens Camera pairs.

**Abstract**— Time-to-Collision (TTC) estimation lies in the core of the forward collision warning (FCW) functionality, which is key to all Automatic Emergency Braking (AEB) systems. Although the success of solutions using frame-based cameras (e.g., Mobileye's solutions) has been witnessed in normal situations, some extreme cases, such as the sudden variation in the relative speed of leading vehicles and the sudden appearance of pedestrians, still pose significant risks that cannot be handled. This is due to the inherent imaging principles of frame-based cameras, where the time interval between adjacent exposures introduces considerable system latency to AEB. Event cameras, as a novel bio-inspired sensor, offer ultra-high temporal resolution and can asynchronously report brightness changes at the microsecond level. To explore the potential of event cameras in the above-mentioned challenging cases, we propose EvTTC, which is, to the best of our knowledge, the first multi-sensor dataset focusing on TTC tasks under high-relative-speed scenarios. EvTTC consists of data collected using standard cameras and event cameras, covering various potential collision scenarios in daily driving and involving multiple collision objects. Additionally, LiDAR and GNSS/INS measurements are provided for the calculation of ground-truth TTC. Considering the high cost of testing TTC algorithms on full-scale mobile platforms, we also provide a small-scale TTC testbed for experimental validation and data augmentation. All the data and the design of the testbed are open sourced, and they can serve as a benchmark that will facilitate the development of vision-based TTC techniques.

**Index Terms**— Computer Vision for Transportation, Event-based Vision, Time to Collision, Collision Avoidance.

This work was supported by the National Key Research and Development Project of China under Grant 2023YFB4706600.

\* Authors contributed equally.

† Corresponding author: Yi Zhou. Email: eeyzhou@hnu.edu.cn.

<sup>1</sup>Neuromorphic Automation and Intelligence Lab (NAIL), School of Robotics, Hunan University, Changsha, China.

<sup>2</sup>School of Engineering, Westlake University, China.

<sup>3</sup>Xidi Zhijia (Hunan) Co., Ltd., Changsha, China.

## MULTIMEDIA MATERIAL

Supplemental video: <https://youtu.be/qJC016GK888>  
EvTTC Benchmark: <https://nail-hnu.github.io/EvTTC/>

## I. INTRODUCTION

Time-to-Collision (TTC) refers to the time it takes for two objects to collide under their current speed. Automated Emergency Braking (AEB) systems, which typically include the Forward Collision Warning (FCW) functionality, are now standard features in automobiles. They apply the vehicle's foundation brakes to prevent a front crash if the driver does not intervene. The key component of FCW is estimating the TTC, which refers to the time it takes for a potential collision under current speed. A large number of technical reports on AEB and FCW have demonstrated that these functionalities reduce front-to-rear crashes by 27%, rear-end collisions by 27%–50%, and rear-end injury crashes by 35%–56% [9], [10], [11], [12].

Compared to LiDAR or radar-based solutions [13], [14], [15], [16], traditional frame-based cameras are a more popular choice due to their low cost. There is extensive research on TTC estimation using traditional cameras [17], [18], [19], [20]. The most common method calculates TTC by analyzing two consecutive images of a monocular camera. The scale of the leading vehicle in the image changes due to its relative motion to the host vehicle, and this variation of scale is used to estimate the TTC. However, this approach is constrained by the frame rate of traditional cameras, which typically operate at 10 Hz in ADAS to balance cost, bandwidth, and power consumption. The resulting 100 ms interval between frames, even before accounting for computation time, can lead

Dataset	Frame Camera		Event Camera		Emergency Break	Groundtruth
	Resolution [pix]	Detection Range [m]	Resolution [pix]	Detection Range [m]		
DR (eye) VE [1]	1920×1080	–	–	–	✗	Driver Attention Map
DADA-2000 [2]	1584×660	–	–	–	✓	Driver Attention Map
Crash to Not Crash [3]	710×400	–	–	–	✓	2D Bounding Box
TSTTC [4]	1024×576	[16-96]	–	–	✗	TTC
MVSEC [5]	752×480	28	346×260	12	✗	Depth, GPS
DSEC [6]	1440×1080	80	640×480	35	✗	Depth, RTK GPS
ViViD++ [7]	1280×1024	53	640×480	50	✗	Depth, RTK GPS
M3ED [8]	1280×800	68	<b>1280×720</b>	65	✗	Depth, RTK GPS
<b>FCWD (Ours)</b>	<b>1920×1200</b>	<b>[160-295]</b>	<b>1280×720</b>	<b>[99-197]</b>	✓	TTC, Depth, RTK GPS

TABLE I: *Comparison of different event camera datasets in driving scenarios.* The symbol “–” indicates not available. Emergency braking represents whether there is a scenario with a rapid decrease in vehicle speed and a small TTC value.

to significant latency in FCW and AEB, especially in high-speed scenarios.

Event-based cameras, inspired by the biological mechanisms of the human visual system, operate differently from traditional frame-based cameras. Rather than capturing entire frames, event-based cameras asynchronously report changes in brightness at individual pixels. This approach offers spatio-temporal sparsity, microsecond-level temporal resolution, and high dynamic range, making event-based cameras well-suited for perception tasks involving rapid motion, such as robotics and autonomous driving [21], [22], [23], [24], [25].

Despite the potential of event-based cameras, research in the field of TTC estimation faces significant challenges, particularly due to the lack of suitable datasets focusing on high relative-speed scenarios. To fill this gap, we present a new dataset (see Fig. 1) that can serve as a benchmark featuring collision scenarios with high relative speed, multiple collision targets, and diverse scenes, facilitating the development and evaluation of TTC estimation methods. The benefits brought by the proposed dataset consist of:

- A diverse set of sequences featuring various targets, such as real vehicles, inflatable vehicles, and dummies, across a wide range of relative speeds, including both routine and challenging situations.
- A low-cost and small-scale TTC testbed that facilitates the generation of quasi-real data at different relative speeds. The design of the testbed is open-source.
- A specific benchmark for the TTC task that can serve as an evaluation platform for the community to test and compare different TTC estimation methods.

*Outline:* The rest of the paper is organized as follows. First, a literature review on datasets of event cameras and those for TTC tasks is provided in Sec. II. Then we provide details of our sensor setup and calibration in Sec. III, followed with descriptions of all the sequences (Sec. IV). Moreover, the design of the small-scale TTC testbed is disclosed in Sec. V. Finally, we establish the TTC benchmark by providing a comprehensive experiment results in Sec. VI, and make the conclusion in Sec. VII.

## II. RELATED WORK

Over the past decade, numerous datasets have been developed to address specific tasks in autonomous driving. Our literature review focuses on two categories: 1) datasets for predicting a traffic collision and 2) outdoor datasets collected using event cameras. Table I provides an overview of these datasets, briefly showcasing the different sensor configurations they use and their different focuses.

The first category focuses on collision risk prediction and TTC estimation. The DR(eye)VE Project [1] and DADA-2000 [2] are notable for their rich data and diverse scenarios. DR(eye)VE provides over 500k frames of normal driving scenes along with driver eye-tracking data, and DADA-2000 includes 2k emergency braking sequences and eye-tracking data from volunteers observing accident videos. These datasets facilitate predicting the risk of a collision by using drivers’ attention data as ground truth. Moreover, [3] provides manually labeled 2D bounding boxes and collision labels, featuring 122 emergency braking scenes and 100 normal driving scenes from YouTube. However, as shown in Tab. I, these datasets lack ground truth of depth and trajectory, limiting their usage in developing TTC estimation algorithms. Among these datasets, the TSTTC [4] dataset is closest to our focus, particularly collected for TTC estimation in driving scenarios. TSTTC is a large-scale dataset with over 200k frames captured from real-world highway and urban environments using monocular cameras with three different focal lengths, covering a detection range of 16-96 meters. It includes ground-truth TTC and 2D/3D bounding boxes, which are crucial for TTC estimation. However, TSTTC mainly focuses on normal driving scenarios with low relative speed between vehicles, and lacks emergency braking under high-speed scenarios, which are essential for evaluating TTC algorithms in extreme conditions.

The second category is those collected using event cameras, which leverages the specialty of event cameras to handle high-speed motion and challenging lighting conditions. Among them, MVSEC [5] is the first stereo event camera dataset, where the stereo rig is handheld or mounted on a mobile platform, such as a drone, an automobile and a motorcycle. Afterwards, Gehrig *et al.* [6] present a large-

Devices	Models	Parameters
8-mm Lens Camera Pair	Prophesee EVKv4	1280×720 1/2.5" FoV: 41°×24°
	FLIR Blackfly S	1920×1200 1/2.3" FoV: 44°×29° Rate: 20Hz
16-mm Lens Camera Pair	Prophesee EVKv4	1280×720 1/2.5" FoV: 22°×12°
	FLIR Blackfly S	1920×1200 1/2.3" FoV: 23°×14° Rate: 20Hz
LiDAR	Livox HAP (TX)	150m @ 10% NIST ±3cm range accuracy FoV: 120°×25° IMU: BMI088
GNSS/INS	CGI-610	Dual-Antenna RTK Rate: 100Hz ±3cm pos. accuracy
	UG005 X1	±2cm/s vel. accuracy

TABLE II: Setup and parameters of the sensor suite.

scale stereo event dataset with higher spatial resolution, better sensor synchronization, and a wide baseline, leading to better depth estimation accuracy. To handle extreme lighting conditions, ViViD++ [7] integrates thermal sensors alongside event cameras, but hardware triggered synchronization is not witnessed. Limited by the immaturity of event cameras at that time, high definition (HD) data are not available in these datasets until the appearance of M3ED [8], which utilizes a Prophesee EVKv4 event camera with a spatial resolution of 1280×720 pixels. In general, these datasets lack specific scenarios and data for the development of TTC tasks.

Different from above-mentioned datasets, the proposed one (called EvTTC) focuses on providing pre-collision data across various speeds and scenarios. The data are collected using a hardware-synchronized sensor suite, which includes two pairs of high-resolution event and RGB cameras with different focal length for covering a larger and wider field of view. Besides, the sensor suite also consists of a LiDAR, an IMU, and a GNSS/INS for providing high-frequency ground-truth information. The pre-collision data involve vehicles and pedestrians, offering comprehensive ground truth of depth, vehicle's pose, TTC, and 2D bounding boxes of front obstacles. As a result, it will fill the gap in high-quality data for TTC tasks under challenging driving conditions.

### III. HARDWARE CONFIGURATION

The setup of the hardware is discussed in this section. Specifically, we disclose the sensors and devices used for recording raw data and ground truth (Sec. III-A), followed by the details of time synchronization across different devices (Sec. III-B) and multi-sensor calibration (Sec. III-C).

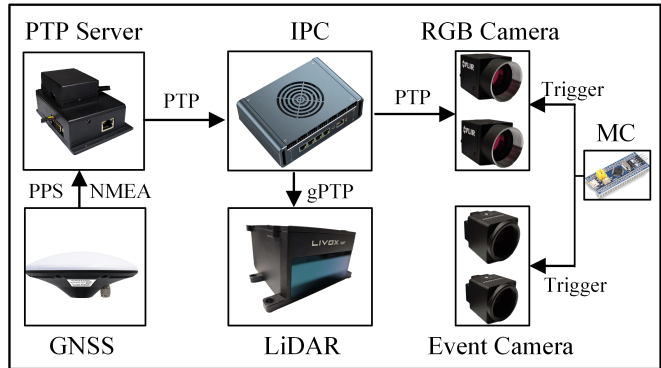


Fig. 2: Illustration of our synchronization scheme.

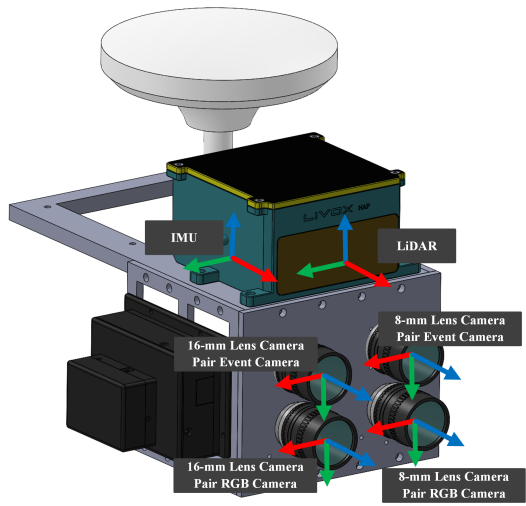


Fig. 3: Illustration of the CAD model of the sensor suite. The axes of all sensors are labeled and color-coded as follows: red for X, green for Y, and blue for Z.

#### A. Sensors

The raw data used for estimating TTC contain RGB images and corresponding event streams. To cover a relatively complete sensing range, we employ two groups of RGB-Event camera pair equipped with lens of different focal length. The camera pair using 8-mm lens consists of an RGB camera and an event camera, and it covers the close sensing range (see (A) in Fig. 1). As a complementary, the camera pair using 16-mm lens is used to cover the distant sensing range (see (B) in Fig. 1). In each pair, the event camera and the RGB camera are rigidly attached with a narrow baseline of 4 cm, and thus, the extrinsic parameters (w.r.t the coordinate system of the sensor suite) can be approximately shared, simplifying data fusion across the two sensor modalities. The employed event camera is Prophesee EVK-v4 (sensor size 1/2.5") that has a spatial resolution of 1280 × 720 pixels. To ensure a similar field of view (FOV), an FLIR Blackfly-S RGB camera (sensor size 1/2.3") with a 1920×1200 resolution is used and equipped with an identical lens. Detailed parameters of each device can be found in Tab. II.

Car-to-Car Rear scenarios			Car-to-Pedestrian scenarios		
CCRs	CCRs-side	CCRm	CPLA	CPNA	CPNAO

Fig. 4: The top-view schematic of the dataset scenarios. The arrow represents the direction of movement. The lateral shadowing of the DCV in the CCRs and CCRm scenarios indicates that data are collected across different lane positions.

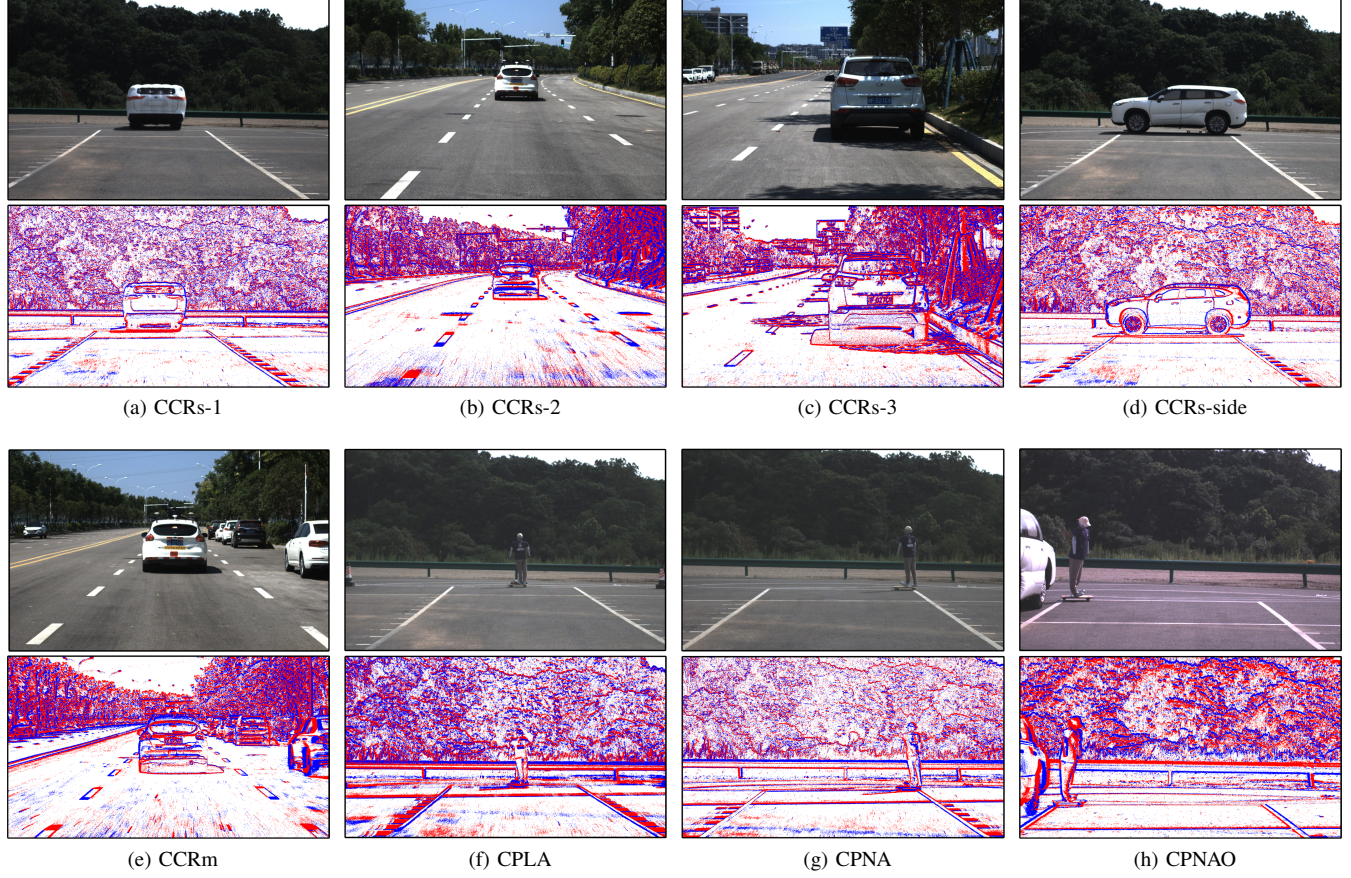


Fig. 5: Illustration of real-world road scenes in our dataset. The top of the first and second rows respectively shows the RGB images for each scenario, while the bottom of the first and second rows respectively presents the accumulated event data for each scenario.

The ground-truth data consists of depth information observed from the host vehicle and the involved two vehicles'

motion status (e.g., position, speed, and orientation, etc). To provide these information, we employ a solid-state LiDAR

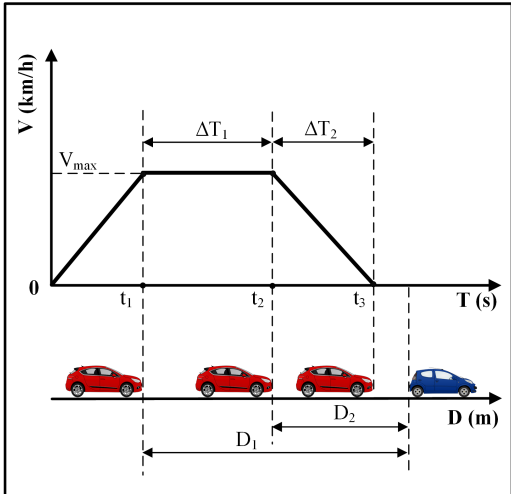


Fig. 6: Parameter definitions in TTC Scenarios.  $\Delta T_1(s)$ : duration at constant speed,  $\Delta T_2(s)$ : braking duration,  $D_1(m)$ : distance to the collision target when the DCV reaches maximum speed,  $D_2(m)$ : distance to the collision target at braking onset.

Seq.	Name	$V_{rel}$	Tier	$\ V_{rel}\ _{max}(\text{km/h})$	$D_1(\text{m})$	$D_2(\text{m})$	$\Delta T_1(\text{s})$	$\Delta T_2(\text{s})$	Total
CCRs-1	low	22.7		50	7	7.4	1.3	3	
	medium	33.5		32	9	2.5	1.5	3	
	high	70.4		109	31	4.2	3.5	3	
CCRs-2	low	14.2		35	12	4.0	3.0	1	
	medium	40.3		58	24	3.0	4.0	1	
	high	57.6		115	38	4.8	5.5	1	
CCRs-3	low	24.1		31	14	2.6	3.5	1	
	medium	41.4		42	25	1.5	3.8	1	
	high	21.2		46	6	7.0	1.1	1	
CCRs-side	medium	35.3		42	12	3.0	2.0	1	
	high	61.9		76	40	2.1	4.5	1	
	low	25.2		57	20	5.5	3.5	3	
CCRm	medium	37.4		34	19	1.5	3.0	3	
	low	24.5		88	6	13.1	1.3	1	
CPLA	medium	41.4		89	10	7.1	1.7	1	
	high	61.6		106	26	4.9	3.5	1	
	low	23.8		92	11	13.0	1.9	1	
CPNA	medium	38.9		108	12	9.1	1.6	1	
	high	61.7		108	23	5.2	2.5	1	
	low	23.7		94	8	14.2	1.9	1	
CPNAO	medium	39.7		104	18	8.2	2.5	1	
	high	55.0		87	42	2.9	4.7	1	

TABLE III: The motion parameters in each TTC scenario.

and two high-performance GNSS/INS units (see Tab. II). A Livox HAP LiDAR is rigidly attached to the two camera pairs and used for collecting ground-truth depth. As for the GNSS/INS devices, a UG005 X1 device is used on the host vehicle, and a CGI-610 device is used on the lead vehicle, both for providing high-frequency motion status of the platform. Note that international organizations of vehicle safety assessment, such as Euro New Car Assessment Program (NCAP), require the motion status of involved vehicles to be collected at a frequency of no lower than 100 Hz. To this end, both GNSS/INS units are configured to provide motion status at 100 Hz.

### B. Time Synchronization

We synchronize all sensors in the sensor suite at the hardware level. To this end, we utilize Precision Timing Protocol (PTP) [26] and the generalized Precision Time Protocol (gPTP) [27], which can provide sub-microsecond synchronization accuracy in the Ethernet.

The time synchronization among all the devices is illustrated in Fig. 2. First, we use a PTP server to synchronize GNSS’s clock with the system clock of the industrial personal computer (IPC). The IPC is then designated as the master clock, using the PTP protocol to synchronize with the RGB cameras. Since the Livox HAP only supports the gPTP protocol, we use gPTP to synchronize between the IPC and the LiDAR. To synchronize the event cameras with the system time, we utilize a micro-controller to generate four synchronization pulses at 20 Hz. These pulses are used to simultaneously trigger the two RGB cameras and the two

event cameras. The RGB and event cameras are configured in external trigger mode. When the RGB camera receives a synchronization pulse, it begins to capture an image and record its timestamp. Meanwhile, the event camera would also be triggered by the synchronization pulse, immediately generating a signal with a timestamp. The temporal offset between the RGB camera and the event camera can be easily calculated as the difference between the two timestamps. In addition, the integrated navigation systems UG005 X1 and CGI-610 are synchronized via their built-in GNSS clocks.

### C. Calibration

We discuss all involved calibration tasks in this part, including the cameras’ intrinsic and extrinsic calibration, extrinsic calibration between cameras and the IMU, and that between cameras and the LiDAR. The precise CAD model of our sensor suite is illustrated in Fig. 3. All calibration results are made available in both YAML and HDF5 formats.

1) *Intrinsic and Extrinsic Calibration of Cameras*: We use the Kalibr toolbox [28] to estimate the intrinsic and extrinsic parameters for the two camera pairs separately. Since the Kalibr toolbox requires image-format data for camera calibration, we utilize the Simple Image Reconstruction library<sup>1</sup> to recover frames from raw event data. For accurate extrinsic parameters estimation, we first synchronize the event and RGB cameras using the synchronization scheme (Sec. III-B), and then perform image reconstruction at the midpoint of each image’s exposure time.

<sup>1</sup>[https://github.com/berndpfrommer/simple\\_image\\_recon](https://github.com/berndpfrommer/simple_image_recon)

2) *Extrinsic Calibration of Cameras and IMU*: For the extrinsic calibration between the cameras and the IMU, we effectively stimulate the sensor suite along the six degrees of freedom of the IMU in front of an *AprilTag* grid pattern and record the corresponding sequences. The Kalibr toolbox is then used to perform the extrinsic calibration.

3) *Extrinsic Calibration of Cameras and LiDAR*: The extrinsic calibration between the RGB cameras and the LiDAR is performed as follows. We first keep the sensor suite static in a structured outdoor scene, and then record multiple point cloud frames along with the corresponding RGB images. The initial guess for the calibration is provided using the CAD statistics of the sensor suite, followed by fine-tuning with the Sensors Calibration toolbox [29] that refines the extrinsic parameters.

#### IV. SEQUENCES OVERVIEW

This section presents a comprehensive overview of the dataset. Following the Euro NCAP AEB test protocol, we collect data for Car-to-Car and Car-to-Pedestrian emergency collision scenarios under various motion conditions (Sec. IV-A), as illustrated in Fig. 4 and Fig. 5. The ground-truth TTC, vehicle poses, and depth information are created by the data from LiDAR and GNSS/INS units (Sec. IV-B).

##### A. Scenarios

1) *Car-to-Car Rear scenarios*: We collect data from two types of scenarios: Car-to-Car Rear stationary (CCRs) and Car-to-Car Rear moving (CCRm). We use two types of real vehicles and a 1:1 scale inflatable vehicle as collision targets, with the latter intended to simulate more realistic collision scenarios while ensuring safety. In the CCRs, when the Global Vehicle Target (GVT) is a real vehicle, it is placed only longitudinally, as shown in Fig. 5(b) and Fig. 5(c). When the GVT is an inflatable vehicle, it is placed both longitudinally and laterally, as illustrated in Fig. 5(a) and Fig. 5(d). In the CCRm, the GVT moves at a constant speed of 20 km/h (see Fig. 5(e)). Additionally, in the CCRs-1 (Fig. 5(a)) and CCRm, the Data Collection Vehicle (DCV) and the GVT occupy different lane positions, including fully aligned, partially offset, and completely offset cases. In all scenarios, the DCV approaches the GVT at speeds ranging from approximately 20 to 60 km/h, as detailed in Fig. 6 and Tab. III.

2) *Car-to-Pedestrian scenarios*: We collect data from three types of scenarios: Car-to-Pedestrian Longitudinal Adult (CPLA), Car-to-Pedestrian Nearside Adult (CPNA), and Car-to-Pedestrian Nearside Adult Obstructed (CPNAO). We select an inflatable dummy as the Adult Pedestrian Target (APT). In the CPLA, the APT is placed in the middle of the road, facing away from the DCV, as shown in Fig. 5(f). In the CPNA, the APT crosses the road at a constant speed, as illustrated in Fig. 5(g). In the CPNAO, the APT suddenly crosses the road from outside the DCV's field of view (see Fig. 5(h)). In all scenarios, the DCV approaches the APT at speeds ranging from approximately 20 to 60 km/h, as shown in Fig. 6 and Tab. III.

Devices	Models	Parameters
Hybird Optical System	Inivation DVXplorer	640×480 1/3.5" FoV: 20°×15°
	DAHENG MER2	1440×1080 FoV: 17°×13° 1/2.9" Rate: 25Hz
Linear Rail system	RXP45-2000	Stroke Pitch: 2000mm Max Speed: 1500mm/s Pos. Accuracy: ±0.05mm Maximum Load: 10kg

TABLE IV: Setup and parameters of the small-scale TTC testbed.

##### B. Ground-truth Generation

1) *TTC*: In the camera coordinate system, the TTC can be calculated as follows:

$$\text{TTC} = \frac{Z}{V_{\text{rel}}} \quad (1)$$

where  $Z$  represents the depth of the collision target in the camera coordinate system, and  $V_{\text{rel}}$  denotes the relative velocity between the DCV and the collision target along the camera's optical axis.

The ground-truth data for depth and vehicle motion status in all sequences are obtained through LiDAR and GNSS/INS units, respectively (see Table II). Specifically, the motion status data for the DCV are collected using the UG005 X1 unit, while the CGI-610 unit is used to collect motion status data for the GVT only in the CCRm scenario, as illustrated in Fig. 5(e). In other scenarios, since the collision target does not move along the camera's optical axis, the position of the collision target can be determined by measuring the distance between the DCV and the target using LiDAR.

With the calibrated extrinsic parameters, all sequence data are transformed into the RGB camera coordinate frame of the 8-mm lens camera pair. The ground-truth TTC is then calculated using the relative depth  $Z$  and relative velocity  $V_{\text{rel}}$  by Eq. 1.

2) *Pose and Depth*: We use the LiDAR odometry FAST-LIO2 [30] to obtain ground-truth poses and velocity-compensated point clouds. For each pose, we extract the relative poses of several preceding and succeeding point cloud frames to generate local point clouds. Next, the Hidden Point Removal (HPR) operator [31] is applied to eliminate occlusion effects in the local point clouds. Finally, the local point clouds are projected into the RGB camera coordinate frames of the 8-mm and 16-mm lens camera pairs to obtain ground-truth depth.

#### V. SMALL-SCALE TESTBED

Considering the gap between synthetic data and real data, the latter is indispensable in the verification of algorithms. However, online evaluation in real-world scenes can be resource intensive. Thus, a design of small-scale TTC testbed, for simulating the emergency scenarios of vehicle collision, is presented.

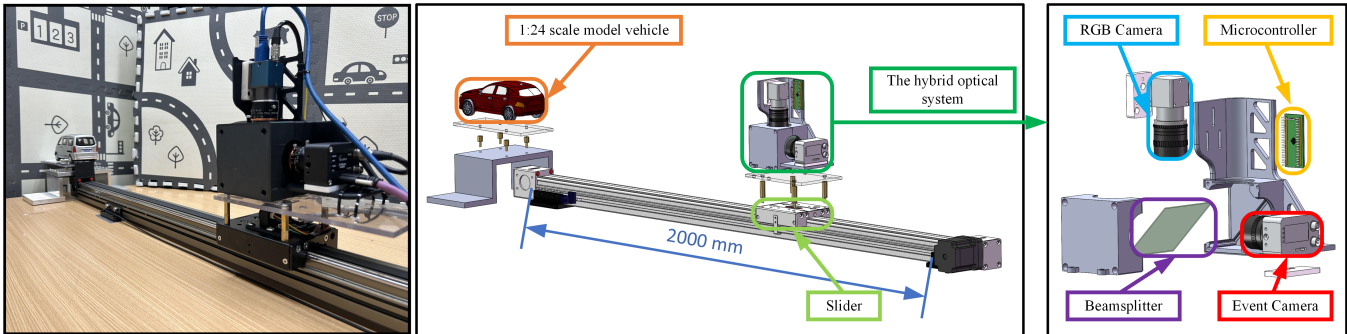


Fig. 7: From left to right: the small-scale TTC testbed, the assembly diagram, and the layout of the hybrid optical system.

Method	CCRs1-low		CCRs1-medium		CCRs1-high		CCRs2-low		CCRs2-medium	
	$e_{TTC}$ (%)	Runtime (s)								
STRTTC [24]	7.54	<u>0.031</u>	9.64	0.026	7.78	0.045	8.15	<u>0.024</u>	11.83	0.024
CMax [32]	<b>2.56</b>	3.833	<b>3.44</b>	3.701	<u>7.39</u>	3.228	<u>5.04</u>	3.246	<u>11.20</u>	3.449
ETTCM [33]	45.11	0.081	44.94	0.081	43.03	0.300	48.83	0.350	52.84	0.098
FAITH [34]	15.15	0.156	20.63	0.155	19.51	0.337	25.83	0.169	47.45	0.191
AEB-Tracker [35]	39.57	<b><math>4.2 \times 10^{-5}</math></b>	42.41	<b><math>3.9 \times 10^{-5}</math></b>	39.04	<b><math>1.1 \times 10^{-5}</math></b>	37.09	<b><math>9.4 \times 10^{-6}</math></b>	43.17	<b><math>7.3 \times 10^{-6}</math></b>
Image's FoE [20]	<u>5.37</u>	0.036	<u>5.12</u>	0.031	<b>1.86</b>	<u>0.041</u>	<b>3.76</b>	0.031	<b>3.85</b>	0.031

Method	CCRs2-high		CCRm-low		CCRm-medium		Slider-750		Slider-1000	
	$e_{TTC}$ (%)	Runtime (s)	$e_{TTC}$ (%)	Runtime (s)	$e_{TTC}$ (%)	Runtime (s)	$e_{TTC}$ (%)	Runtime (s)	$e_{TTC}$ (%)	Runtime (s)
STRTTC [24]	13.68	<u>0.028</u>	9.87	0.031	<u>10.36</u>	0.023	<u>8.95</u>	0.015	12.43	0.016
CMax [32]	11.10	<u>3.826</u>	9.27	3.658	<u>14.73</u>	<u>3.657</u>	<b>4.16</b>	0.85	<b>2.74</b>	0.93
ETTCM [33]	49.46	0.127	71.05	0.059	58.00	0.121	18.99	0.498	15.20	0.191
FAITH [34]	49.62	0.165	75.78	0.116	56.26	0.11	34.45	0.186	47.94	0.233
AEB-Tracker [35]	42.43	<b><math>6 \times 10^{-6}</math></b>	26.95	<b><math>1 \times 10^{-5}</math></b>	35.99	<b><math>1.1 \times 10^{-5}</math></b>	157.88	<b><math>1 \times 10^{-5}</math></b>	165.56	<b><math>7.8 \times 10^{-6}</math></b>
Image's FoE [20]	<b>2.92</b>	0.031	<b>5.60</b>	<u>0.027</u>	<b>3.86</b>	0.026	11.35	<u>0.013</u>	<u>7.55</u>	<u>0.012</u>

TABLE V: Performance of multiple TTC estimation algorithms. Best and second best results are **highlighted** and underlined, respectively.

The testbed consists of a hybrid optical system [36], a linear rail and a 1:24 scale model vehicle. Fig. 7 illustrates the platform setup, and Tab. IV specifies the device parameters. Specifically, the hybrid optical system comprises an DVX-explorer event camera, an RGB camera, and a beam splitter. The beam splitter divides the incoming light into two paths, ensuring that both cameras share a unified field of view, facilitating pixel-level correspondence between the event and RGB cameras. To achieve precise time synchronization, a micro-controller is used to generate two synchronized 25 Hz pulse signals, which are employed to simultaneously trigger both cameras. The linear rail has an effective travel distance of 2 meters, with a control system that includes a servomotor, a driver, and an STM32 development board. Besides, a 1:24 scale model vehicle is positioned in front of the camera, being used as the potential collision target. The hybrid optical system is rigidly mounted on the slider, which can be propelled towards the target under accurate control of speed. The ground-truth TTC is calculated based on the velocity and relative displacement measured by the motor encoder.

## VI. TTC BENCHMARK

With the above dataset and testing platform, we provide a publicly accessible benchmark to the community. To this end, we evaluate a number of TTC estimation algorithms, including STRTTC [24], CMax [32], ETTCM [33], FAITH [34],

AEB-Tracker [35] and Image's FOE [20], using our dataset. All evaluation results are obtained by averaging over multiple runs. The results of these algorithms are presented in Tab. V.

STRTTC [24] demonstrates robust performance under various conditions, attributed to its resilient sampling strategy and efficient initialization scheme. In contrast, CMax [32] achieves higher accuracy by utilizing all events within the bounding box, enhancing the signal-to-noise ratio. However, its nonlinear least-squares optimization adds computational complexity, with processing 3e5 events typically taking around 3 seconds. As an event-based incremental methodology, ETTCM [33] does not scale well with input data generated per unit time. FAITH [34] replaces optical flow with normal flow for TTC estimation, leading to worse accuracy. AEB-Tracker [35] achieves exceptionally high computational efficiency, reaching up to 10 kHz. However, under conditions with significant background noise, the algorithm requires a low-frequency detector to identify regions (e.g., two taillights) capable of generating event blobs. Image's FOE [20] achieves high accuracy and efficiency across all sequences; Nevertheless, its performance is constrained by the limitations of standard cameras (e.g., data latency, motion blur).

## VII. CONCLUSION

We present an event camera dataset, called EvTTC, for the task of time-to-collision estimation in autonomous driving. It

consists of data captured using frame-based and event-based cameras, covering various scenarios of potential collision in daily driving. High-precision external reference signals are also provided for ground truth, and a benchmark of event-based TTC is established. Besides, a small-scale TTC testbed for experimental validation and data augmentation is presented. We wish the release of EvTTC can facilitate the development of forward collision warning techniques using event cameras.

#### ACKNOWLEDGMENT

We thank Javier Hidalgo-Carrió and Davide Scaramuzza for releasing the design of the Beamsplitter [36], based on which we build our FCW system. We thank Mr. Yanggang Sheng and Mr. Junkai Niu for the help in the data collection.

#### REFERENCES

- [1] A. Palazzi, D. Abati, F. Solera, R. Cucchiara, *et al.*, “Predicting the driver’s focus of attention: the dr (eye) ve project,” *IEEE transactions on pattern analysis and machine intelligence*, vol. 41, no. 7, pp. 1720–1733, 2018.
- [2] J. Fang, D. Yan, J. Qiao, J. Xue, H. Wang, and S. Li, “Dada-2000: Can driving accident be predicted by driver attentionf analyzed by a benchmark,” in *2019 IEEE Intelligent Transportation Systems Conference (ITSC)*. IEEE, 2019, pp. 4303–4309.
- [3] H. Kim, K. Lee, G. Hwang, and C. Suh, “Crash to not crash: Learn to identify dangerous vehicles using a simulator,” in *Proceedings of the AAAI Conference on Artificial Intelligence*, vol. 33, no. 01, 2019, pp. 978–985.
- [4] Y. Shi, Z. Huang, Y. Yan, N. Wang, and X. Guo, “Tsttc: A large-scale dataset for time-to-contact estimation in driving scenarios,” *arXiv preprint arXiv:2309.01539*, 2023.
- [5] A. Z. Zhu, D. Thakur, T. Özslan, B. Pfrommer, V. Kumar, and K. Daniilidis, “The multivehicle stereo event camera dataset: An event camera dataset for 3d perception,” *IEEE Robotics and Automation Letters*, vol. 3, no. 3, pp. 2032–2039, 2018.
- [6] M. Gehrig, W. Aarents, D. Gehrig, and D. Scaramuzza, “Dsec: A stereo event camera dataset for driving scenarios,” *IEEE Robotics and Automation Letters*, 2021.
- [7] A. J. Lee, Y. Cho, Y.-s. Shin, A. Kim, and H. Myung, “Vivid++: Vision for visibility dataset,” *IEEE Robotics and Automation Letters*, vol. 7, no. 3, pp. 6282–6289, 2022.
- [8] K. Chaney, F. Cladera, Z. Wang, A. Bisulco, M. A. Hsieh, C. Korpela, V. Kumar, C. J. Taylor, and K. Daniilidis, “M3ed: Multi-robot, multi-sensor, multi-environment event dataset,” in *Proceedings of the IEEE/CVF Conference on Computer Vision and Pattern Recognition*, 2023, pp. 4015–4022.
- [9] J. B. Cicchino, “Effectiveness of forward collision warning and autonomous emergency braking systems in reducing front-to-rear crash rates,” *Accident Analysis & Prevention*, vol. 99, pp. 142–152, 2017.
- [10] B. Fildes, M. Keall, N. Bos, A. Lie, Y. Page, C. Pastor, L. Pennisi, M. Rizzi, P. Thomas, and C. Tingvall, “Effectiveness of low speed autonomous emergency braking in real-world rear-end crashes,” *Accident Analysis & Prevention*, vol. 81, pp. 24–29, 2015.
- [11] I. Isaksson-Hellman and M. Lindman, “Evaluation of rear-end collision avoidance technologies based on real world crash data,” *Proceedings of the Future Active Safety Technology Towards zero traffic accidents (FASTzero)*, Gothenburg, Sweden, pp. 9–11, 2015.
- [12] M. Rizzi, A. Kullgren, and C. Tingvall, “Injury crash reduction of low-speed autonomous emergency braking (aeb) on passenger cars,” in *International Research Council on the Biomechanics of Injury (IRCOBI 2014)*. International Research Council on the Biomechanics of Injury, 2014, pp. 656–665.
- [13] M. Gawande, P. Rajalakshmi, *et al.*, “Autonomous emergency breaking (aeb) evaluation for indian traffic scenarios using gps and lidar data,” in *2022 IEEE IAS Global Conference on Emerging Technologies (GlobConET)*. IEEE, 2022, pp. 655–660.
- [14] M. Bosnak and I. Skrjanc, “Efficient time-to-collision estimation for a braking supervision system with lidar,” in *2017 3rd IEEE International Conference on Cybernetics (CYBCONF)*. IEEE, 2017, pp. 1–6.
- [15] M. Kotur, N. Lukić, M. Krunić, and Ž. Lukač, “Camera and lidar sensor fusion for 3d object tracking in a collision avoidance system,” in *2021 Zooming Innovation in Consumer Technologies Conference (ZINC)*. IEEE, 2021, pp. 198–202.
- [16] K. Venkatesha, A. Vengadarajan, and U. Singh, “Detection mechanism for vehicle collision avoidance using mmwave radar,” in *2023 IEEE International Conference on Electronics, Computing and Communication Technologies (CONECT)*. IEEE, 2023, pp. 1–5.
- [17] E. Dagan, O. Mano, G. P. Stein, and A. Shashua, “Forward collision warning with a single camera,” in *IEEE Intelligent Vehicles Symposium, 2004*. IEEE, 2004, pp. 37–42.
- [18] F. Meyer and P. Bouthemy, “Estimation of time-to-collision maps from first order motion models and normal flows,” in *1992 11th IAPR International Conference on Pattern Recognition*, vol. 1. IEEE Computer Society, 1992, pp. 78–82.
- [19] A. Negre, C. Braillon, J. L. Crowley, and C. Laugier, “Real-time time-to-collision from variation of intrinsic scale,” in *Experimental Robotics: The 10th International Symposium on Experimental Robotics*. Springer, 2008, pp. 75–84.
- [20] S. Stabinger, A. Rodriguez-Sánchez, and J. Piater, “Monocular obstacle avoidance for blind people using probabilistic focus of expansion estimation,” in *2016 IEEE Winter Conference on Applications of Computer Vision (WACV)*. IEEE, 2016, pp. 1–9.
- [21] D. Falanga, K. Kleber, and D. Scaramuzza, “Dynamic obstacle avoidance for quadrotors with event cameras,” *Science Robotics*, vol. 5, no. 40, p. eaaz9712, 2020.
- [22] H. Rebecq, T. Horstschaefer, and D. Scaramuzza, “Real-time visual-inertial odometry for event cameras using keyframe-based nonlinear optimization,” 2017.
- [23] X. Lu, Y. Zhou, and S. Shen, “Event-based visual inertial velocimeter,” *Robotics: Science and Systems (RSS)*, 2024.
- [24] J. Li, B. Liao, X. Lu, P. Liu, S. Shen, and Y. Zhou, “Event-aided time-to-collision estimation for autonomous driving,” in *European Conference on Computer Vision*. Springer, 2025, pp. 57–73.
- [25] D. Gehrig and D. Scaramuzza, “Low-latency automotive vision with event cameras,” *Nature*, vol. 629, no. 8014, pp. 1034–1040, 2024.
- [26] IEEE Std 1588-2019 (Revision of IEEE Std 1588-2008), “IEEE Standard for a Precision Clock Synchronization Protocol for Networked Measurement and Control Systems,” pp. 1–499, 2020.
- [27] IEEE Std 802.1AS-2020 (Revision of IEEE Std 802.1AS-2011), “IEEE Standard for Local and Metropolitan Area Networks—Timing and Synchronization for Time-Sensitive Applications,” pp. 1–421, 2020.
- [28] P. Furgale, J. Rehder, and R. Siegwart, “Unified temporal and spatial calibration for multi-sensor systems,” in *2013 IEEE/RSJ International Conference on Intelligent Robots and Systems*. IEEE, 2013, pp. 1280–1286.
- [29] G. Yan, Z. Liu, C. Wang, C. Shi, P. Wei, X. Cai, T. Ma, Z. Liu, Z. Zhong, Y. Liu, M. Zhao, Z. Ma, and Y. Li, “Opencalib: A multi-sensor calibration toolbox for autonomous driving,” *arXiv preprint arXiv:2205.14087*, 2022.
- [30] W. Xu, Y. Cai, D. He, J. Lin, and F. Zhang, “Fast-lio2: Fast direct lidar-inertial odometry,” *IEEE Transactions on Robotics*, vol. 38, no. 4, pp. 2053–2073, 2022.
- [31] S. Katz, A. Tal, and R. Basri, “Direct visibility of point sets,” in *ACM SIGGRAPH 2007 papers*, 2007, pp. 24–es.
- [32] G. Gallego, H. Rebecq, and D. Scaramuzza, “A unifying contrast maximization framework for event cameras, with applications to motion, depth, and optical flow estimation,” in *Proceedings of the IEEE conference on computer vision and pattern recognition*, 2018, pp. 3867–3876.
- [33] U. M. Nunes, L. U. Perrinet, and S.-H. Ieng, “Time-to-contact map by joint estimation of up-to-scale inverse depth and global motion using a single event camera,” in *Proceedings of the IEEE/CVF International Conference on Computer Vision*, 2023, pp. 23 653–23 663.
- [34] R. Dinaux, N. Wessendorp, J. Dupeyroux, and G. C. De Croon, “Faith: Fast iterative half-plane focus of expansion estimation using optic flow,” *IEEE Robotics and Automation Letters*, vol. 6, no. 4, pp. 7627–7634, 2021.
- [35] Z. Wang, T. Molloy, P. van Goor, and R. Mahony, “Asynchronous blob tracker for event cameras,” *IEEE Transactions on Robotics*, 2024.
- [36] J. Hidalgo-Carrió, G. Gallego, and D. Scaramuzza, “Event-aided direct sparse odometry,” in *Proceedings of the IEEE/CVF Conference on Computer Vision and Pattern Recognition*, 2022, pp. 5781–5790.